The Astrophysical Journal, 728:147 (6pp), 2011 February 20 doi:10.1088/0004-637X/728/2/147

A CORONAL SEISMOLOGICAL STUDY WITH STREAMER WAVES

Y. Chen[1], S. W. Feng[1], B. Li[1], H. Q. Song[1], L. D. Xia[1], X. L. Kong[1], and Xing Li[2]
[1] Shandong Provincial Key Laboratory of Optical Astronomy and Solar-Terrestrial Environment, School of Space Science and Physics, Shandong University at Weihai, Weihai 264209, China; yaochen@sdu.edu.cn
[2] Department of Physics, University of Wales, Aberystwyth, SY23 3BZ, UK
Received 2010 September 29; accepted 2010 December 15; published 2011 February 1

ABSTRACT

We present a novel method to evaluate the Alfvén speed and the magnetic field strength along the streamer plasma sheet in the outer corona. The method is based on recent observations of streamer waves, which are regarded as the fast kink body mode carried by the plasma sheet structure and generated upon the impact of a fast coronal mass ejection (CME) on a nearby streamer. The mode propagates outward with a phase speed consisting of two components. One is the phase speed of the mode in the plasma rest frame and the other is the speed of the solar wind streaming along the plasma sheet. The former can be well represented by the Alfvén speed outside the plasma sheet, according to a linear wave dispersion analysis with a simplified slab model of magnetized plasmas. The radial profiles of the Alfvén speed can be deduced with constraints put on the speed of the solar wind, which is done by making use of the measurements of streamer blobs flowing passively in the wind. The radial profiles of the strength of the coronal magnetic field can be depicted once the electron density distribution is specified, this is done by inverting the observed polarized brightness data. Comparing the diagnostic results corresponding to the first wave trough and the following crest, we find that both the Alfvén speed and magnetic field strength at a fixed distance decline with time. This is suggestive of the recovering process of the CME-disturbed corona.

Key words: magnetohydrodynamics (MHD) – Sun: corona – Sun: coronal mass ejections (CMEs) – waves

Online-only material: color figure

1. INTRODUCTION

The magnetic field plays an important role in physical processes occurring at all relevant coronal heights. From the photosphere to the inner corona, the strength of the magnetic field can be measured by the conventional Zeeman splitting technique. However, in the outer corona beyond, say, 1.2–1.5 $R_\odot$, the field gets too weak to be measured directly. Indirect methods available at present are mostly based on numerical extrapolations or various types of radio techniques.

With the extrapolation method, the coronal magnetic field distributions are resolved numerically by extrapolating the measured photospheric magnetic field, making use of potential field (Schatten et al. 1969; Schrijver & Derosa 2003), linear or nonlinear force-free field assumptions (e.g., Yan & Sakurai 2000; Wiegelmann 2008; He & Wang 2008), or solving the full set of magnetohydrodynamic (MHD) equations (e.g., Linker et al. 1999). There also exist various types of techniques employing radio emissions to derive the coronal magnetic field strength. The first one utilizes the well-known Faraday rotation effect acting on a linearly polarized radio signal passing through coronal structures. Signals from both extragalactic radio sources (Sakurai & Spangler 1994; Mancuso & Spangler 1999, 2000; Spangler 2005; Ingleby et al. 2007) and spacecraft radio emitters (Pätzold et al. 1987) have been analyzed over the past decades. To use this method, one needs to determine independently the coronal electron density distribution and the geometry of the magnetic field. The method applies to the heliocentric distance range of 3–10 $R_\odot$. The second one is based on the band-splitting phenomenon observed during Type-II radio bursts related to shocks driven by coronal mass ejections (CMEs; Smerd et al. 1974, 1975; Vrsnak et al. 2002; Cho et al. 2007). The phenomenon is interpreted as plasma emissions from downstream and upstream of the shock front at different frequencies. To implement this method one needs to apply the MHD shock theory and presume the value of the plasma β, the shock geometry, as well as the coronal electron density distribution. The method works for the heliocentric distance range of 1.5–3 $R_\odot$. The third method makes use of observations of circularly polarized thermal radio emissions (Sastry 2009), which was recently explored to estimate the magnetic field strength in coronal streamers at heliocentric distances of 1.5 and 1.7 $R_\odot$ by Ramesh et al. (2010). In this paper, we present a novel seismological method to evaluate the strength of the magnetic field in the outer corona.

Coronal seismology is a way to diagnose the physical parameters of the corona with observational and MHD theoretical analyses of waves and oscillations. Here, we present a seismological study to derive the Alfvén speed and magnetic field strength with the use of the so-called streamer waves, reported recently by Chen et al. (2010, referred to as Paper I hereafter). The waves were observed by the Large Angle and Spectrometric Coronagraph (LASCO) and generated as the aftermath of the CME–streamer interaction event dated on 2004 July 6. The wave properties such as the wavelength, period, and phase speed, as well as the possibility of deriving the magnetic field strength with this wave, are already presented in Paper I. Here, we briefly discuss the theoretical basis and procedures of implementing the concerned seismological study.

The waves are regarded as the fast kink body mode carried by the plasma sheet structure of a streamer. The phase speed of the mode has two contributions. One is the phase speed of the mode in the plasma rest frame and the other is the speed of the solar wind streaming along the plasma sheet. The former can be well approximated by the exterior Alfvén speed according to a linear wave dispersion analysis, which will be carried out in the Appendix of this paper. As a result, the radial profile of the Alfvén speed and that of the magnetic

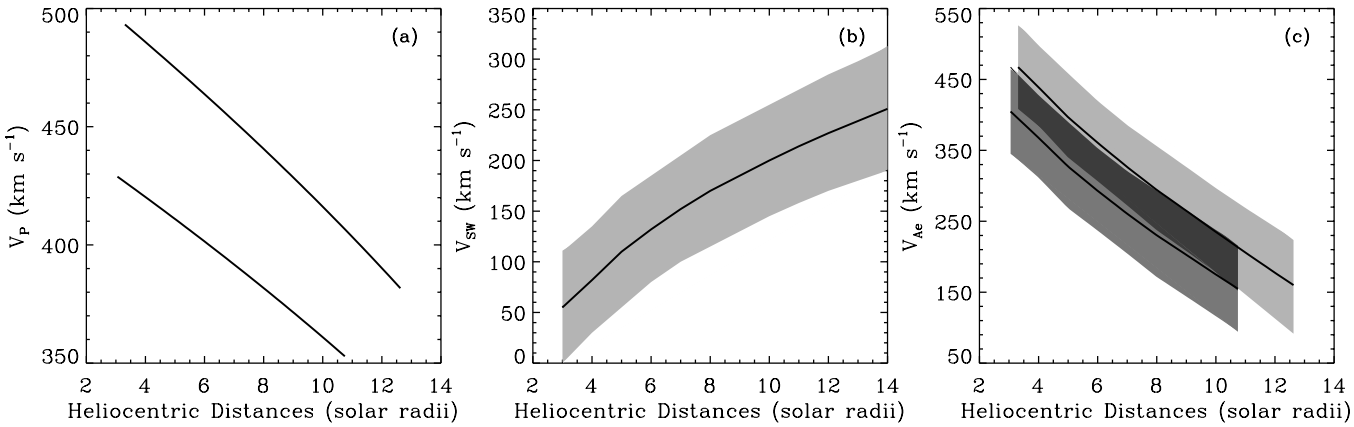

Figure 1. (a) Radial profiles of propagation speeds of phases P1 and P2 of the streamer wave observed on 2004 July 6 (taken from Paper I); (b) speed variations of the solar wind along the streamer plasma sheet, deduced from the blob measurements (taken from Wang et al. 2000), the solid line represents the mean speed; (c) light and dark areas represent variation ranges of the exterior Alfvén speed v_{Ae} corresponding to wave phases P1 and P2, the solid lines are v_{Ae} associated with the mean wind speed.

field strength can be deduced given the speed and density of the solar wind plasmas. In Paper I, by taking these solar wind parameters from a simplified two-dimensional MHD model accounting for streamers, current-plasma sheets, and slow-fast winds developed by Chen & Hu (2001), the magnetic field strengths at 5 and 10 $R_\odot$ are evaluated. It should be pointed out that the seismological study in Paper I is rather preliminary and incomplete. The purpose of this paper is to further improve and complete the study.

It will be improved in the following three aspects. First, in Paper I the Alfvén speed in the region surrounding the plasma sheet is set to be equal to the phase speed of the kink mode in the plasma rest frame. In this paper, we will conduct a parameter study on dispersion relation of the fast kink body mode with a simplified slab model of magnetized plasmas given by Edwin & Roberts (1982), making use of different sets of coronal parameters prescribed according to available observational diagnoses and theoretical modelings. From the study, we deduce the appropriate connection of the kink mode phase speed to the exterior Alfvén speed. Second, we employ available observational results to put constraints on the flow speed and number density of the solar wind along the plasma sheet. The former will be constrained by measurements of plasma blobs, which are structures released intermittently through streamer cusps and flowing outward passively in the wind along the plasma sheet. The feasibility of using blobs to yield the wind speed has been discussed in several papers (Sheeley et al. 1997; Wang et al. 1998, 2000; Song et al. 2009; and Chen et al. 2009) and will not be repeated here. The number density will be derived by inversion of the polarized brightness (pB) measurements given by LASCO at the time prior to the CME–streamer interaction event. Third, in Paper I only the magnetic field strengths at two distances were estimated, while in this paper two sets of radial profiles of both the Alfvén speed and magnetic field strength in the heliocentric range of 3–10 $R_\odot$, corresponding to two subsequent wave phases, will be presented. This will provide the information on not only spatial but also temporal variations of the two critical coronal parameters.

In the following section, we show major relevant results on streamer waves of Paper I and present the radial profiles of the Alfvén speed. The strength of the coronal magnetic field will be deduced in Section 3. Conclusions and discussion are given in Section 4, and the associated wave dispersion analysis is presented in the Appendix.

2. PHASE SPEED OBSERVATIONS AND THE DEDUCED PROFILES OF THE ALFVÉN SPEED

Observational features of the streamer wave event dated on 2004 July 6 were described in Paper I. The wave profiles, as well as heliocentric distances of five propagating wave troughs/crests, were extracted from the running difference images of the white-light coronagraph observations. The corresponding phase speeds were derived with a second-order polynomial fitting to the relevant distance–time profiles. In Figure 1(a), we re-show the radial profiles of the first two sets of phase speeds, corresponding to the outward propagation of the first observed wave trough and the following crest which are referred to as P1 and P2 hereafter. These phase speeds will be used for further seismological studies. From Figure 1(a), we see that the phase speed declines with increasing distance, e.g., for P1 (P2), the speed decreases from 493 (428) km s^{-1} at 3.3 (3.05) $R_\odot$ to 474 (411) at 5 $R_\odot$ and 415 (361) km s^{-1} at 10 $R_\odot$. At a fixed distance, P1 moves faster than P2 by about 60 km s^{-1}. This difference in phase speeds was employed to understand the increase of wavelength during the propagation of the streamer wave.

The observed streamer wave was interpreted as the fast kink body mode carried by the thin-sheet structure of the streamer stalk. To deduce the mode phase speed in the plasma rest frame (v_k), one has to determine the speed of the mean flow through which the mode propagates. As mentioned previously, velocity measurements given by about 80 blobs and shown in Figure 1(b) as shadows are used to provide constraints on the speed of the solar wind along the plasma sheet (Wang et al. 2000). The solid line inside the shadow area represents the mean solar wind velocity. Subtracting the shown solar wind velocities from the measured phase speeds in Figure 1(a), one gets v_k. To deduce the concerned Alfvén speed from v_k, one still needs to determine their relationship. This is done in the Appendix with a parameter study on the dispersion relation of the fast kink body mode in a slab configuration of magnetized plasmas under local approximations (Equation (11) of Edwin & Roberts 1982). From the study, we conclude that it is appropriate to approximate the Alfvén speed in the region surrounding the plasma sheet (v_{Ae}) by the equation $v_{Ae} = v_k/\alpha$, where α is fixed to be 0.92.

The external Alfvén speed v_{Ae} thus obtained is presented in Figure 1(c) with light and dark shadow areas corresponding to phases P1 and P2, respectively. The solid lines are associated with the mean wind speed as plotted in Figure 1(b). It can be seen

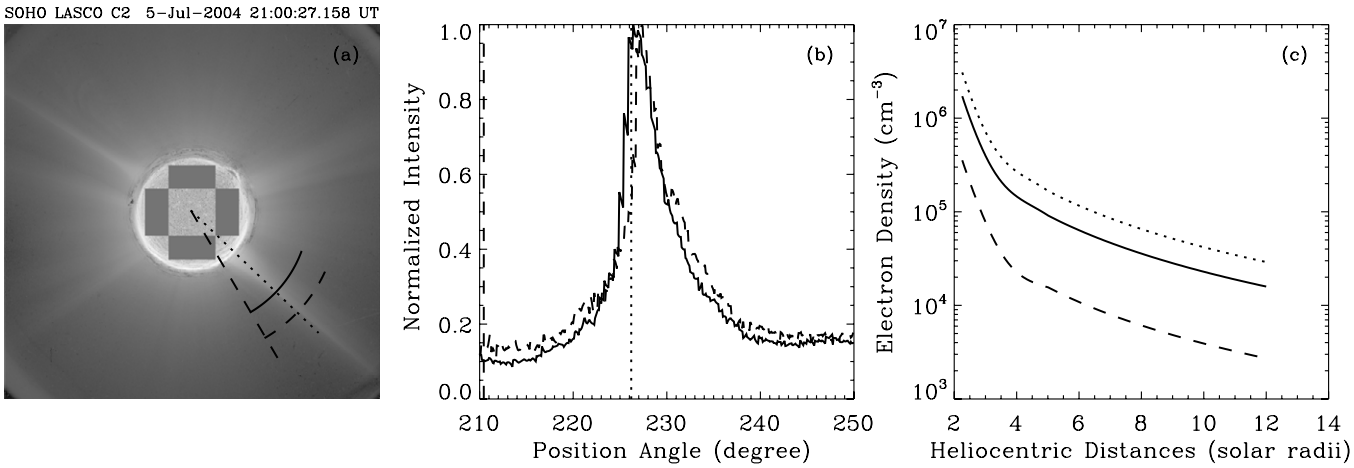

Figure 2. (a) The pB distribution observed by LASCO, the two arcs are at heliocentric distances of 4 and 5 $R_\odot$, the dotted (dashed) line denotes a specific P.A. of 226° (211°); (b) the solid (dashed) line presents the latitudinal profiles of pB at 4 (5) $R_\odot$, the vertical lines are the P.A.s shown in panel (a); (c) dotted and dashed lines are the electron number densities given by the pB inversion program for P.A. = 226° and 211°, respectively, the solid line shows the average of them. Densities beyond 5 $R_\odot$ are determined according to an r^{-2} dependence.

that v_{Ae} decreases from 408–526 km s^{-1} at 3.3 $R_\odot$ to 338–457 (175–294) km s^{-1} at 5 (10) $R_\odot$ for P1 and from 345–464 km s^{-1} at 3.05 $R_\odot$ to 266–385 (116–235) km s^{-1} at 5 (10) $R_\odot$ for P2. Using the same magnitude of the wind speed, the difference between the P1 and P2 v_{Ae} is about 60 km s^{-1}. The timing difference between the two phases is about half of the wave period, i.e., about half an hour. Therefore, it is suggested that the above difference of v_{Ae} is a result of the recovering process of the CME-disturbed corona during this interval.

3. RADIAL PROFILES OF THE MAGNETIC FIELD STRENGTH

In the above section, we deduce the radial profiles of the Alfvén speed in the region surrounding the plasma sheet. To determine the corresponding magnetic field strength, one needs to specify the plasma density distribution in the region. This is done through inversion of the LASCO pB data, as mentioned earlier. Since the pB data were recorded at 21:00 on 2004 July 6 when the streamer already got deflected and waved away from its equilibrium, it is not possible to determine a sole direction of the axis. We therefore make use of the pB data obtained one day earlier for the purpose of inversion. This is equivalent to assuming that the streamer density does not change appreciably during the day from 21:00 July 5 to 21:00 July 6.

Before showing the electron density profiles, we first discuss the latitudinal variation of the pB data plotted in Figure 2(b) for 4 (solid) and 5 (dashed) $R_\odot$. From this figure, we have determined the angular width of the plasma sheet to be about 3° (see the Appendix). It can be seen that outside of the plasma sheet, the pB value, or most equivalently the electron density at the same height, decreases gradually in a range of about 10°. This inhomogeneous density distribution outside the plasma sheet is different from what was assumed in the simplified slab model employed in the Appendix, where densities distribute uniformly in both the interior and exterior of the plasma sheet. To reconcile this discrepancy, we suggest that the exterior parameters n_e, v_{Ae}, as well as B_e be investigated and should be regarded as effective averages of the inhomogeneously distributed parameters outside the realistic plasma sheet.

Keeping this in mind, we select two position angles (P.A.s) 226° and 211°, as already marked in Figures 2(a) and (b). The former P.A. lies near the streamer axis and the latter is placed about 15° away. The electron density profiles along the P.A.s below 5 $R_\odot$ given by the pB inversion method and those beyond determined by assuming the r^{-2} dependence are shown in Figure 2(c) with dashed (226°) and dotted (211°) lines. Along P.A. = 226° the electron density equals 7.19×10^5 (1.67×10^5) cm^{-3} at 3 (5) $R_\odot$ and along P.A. = 211° the electron density is much smaller being 7.82×10^4 (1.56×10^4) cm^{-3} at the same distance. The solid line represents the average of the two densities, which are approximately half of the densities along the streamer axis, being 3.99×10^5 (9.12×10^4) cm^{-3} also at 3 (5) $R_\odot$. According to the above discussion, we take the average density to be n_e, which is then substituted into the obtained v_{Ae} values to estimate the strength of the magnetic field B_e. The limitations of this approach will be discussed in the following section.

Radial profiles of B_e corresponding to P1 and P2 are shown in Figure 3 with light (upper) and dark (lower) shadow areas, respectively. It can be seen that B_e varies in between 0.096 and 0.123 G at 3.3 $R_\odot$ and decreases to 0.047–0.064 (0.012–0.020) G at 5 (10) $R_\odot$ for P1, and decreases from 0.096–0.129 G at 3.05 $R_\odot$ to 0.037–0.053 (0.008–0.016) G at 5 (10) $R_\odot$ for P2. The variation of B_e at a fixed distance for a certain wave phase is a straightforward result of the large range of the solar wind velocity used in the deduction of v_{Ae}. A larger B_e (v_{Ae}) corresponds to a slower solar wind. Thus, the impact of the velocity of the solar wind along the plasma sheet, which is not yet directly measurable, on our diagnostic results can be directly read from the figures. The solid lines in the middle of the shadow areas denote B_e distributions associated with the mean velocity of the solar wind. For comparison, we also plot the magnetic field strength profiles decreasing according to the r^{-2} dependence. We see that deviations from radial expansion are not significant, so we suggest that the deduced magnetic field expands basically radially.

The magnetic field corresponding to P1 is generally stronger than that corresponding to P2 if identical solar wind speeds are used to deduce the field strength. The discrepancies of the two sets of field strength can be regarded as the field temporal change over the interval of half an hour. The change is suggested to be a result of the recovering process of the CME-disturbed corona, as proposed to explain the v_{Ae} change in the above section. It

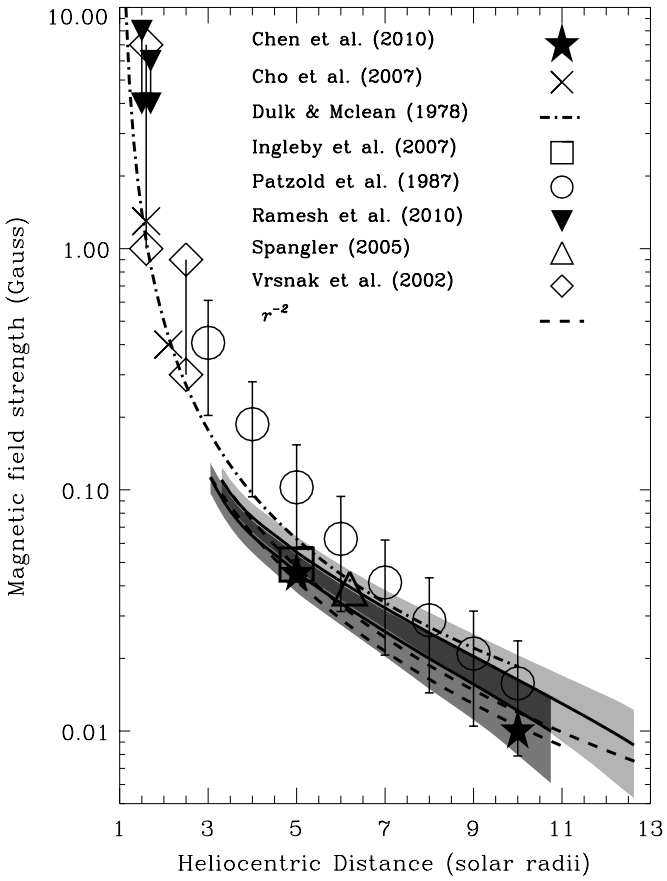

Figure 3. Areas in shadow present the deduced radial profiles of the strength of the magnetic field along the plasma sheet. The upper (lower) one is associated with P1 (P2). The solid lines correspond to the mean solar wind speed shown in Figure 1(b), the dashed lines show the variation of the field strength assuming the r^{-2} dependence. Various symbols represent other estimates on the coronal magnetic field strength.

should be pointed out that for P1 and P2 we have used the same set of wind parameters, while they do change temporally with the recovering process. This contributes to the uncertainty of our results. This will be further discussed in the following section.

In Figure 3, we also show other diagnoses on the magnetic field strength in the corona with various symbols. The preliminary results of B_e of Paper I are shown as stars, which are 0.045 (0.01) G at 5 (10) $R_\odot$ based on the P2 phase speed measurement and the solar wind model of Chen & Hu (2001). Other results are mostly obtained employing radio methods. To be specific, the strength–distance relationship in the heliocentric range of 1.02–10 $R_\odot$ above active regions (dot-dashed line) given by Dulk & McLean (1978) is mainly based on radio burst observations, the results of Vrsnak et al. (2002) and Cho et al. (2007) presented as crosses and diamonds are deduced using the band-splitting phenomenon of Type-II radio bursts, the results of Pätzold et al. (1987) plotted as open circles with error bars are given by the Faraday rotation measurement of radio signals emitted by the Helios spacecraft, and similar results associated with the extragalactic radio signals are included as triangles (Spangler 2005) and squares (Ingleby et al. 2007) for heliocentric distances of 6.2 $R_\odot$ (0.039 G) and 5 $R_\odot$ (0.046–0.052 G), respectively. The latest results obtained by Ramesh et al. (2010) employing the low-frequency circularly polarized radio emission at 1.5 (6 ± 2 G) and 1.7 (5 ± 1 G) $R_\odot$ inside a streamer structure are given as solid inverse triangles. We note that the above list of diagnoses of the coronal field strength is incomplete and there exist many other estimates (see, e.g., references in Vrsnak et al. 2002). From Figure 3, it can be seen that the magnitude and variation trend of our magnetic field strength in the region surrounding the plasma sheet are basically in line with others.

4. CONCLUSIONS AND DISCUSSION

In this paper, we provide a novel method to diagnose the Alfvén speed and magnetic field strength in the corona based on the observations of streamer waves, which propagate with phase speeds consisting of two components. One is the speed of the wave mode in the plasma rest frame and the other is the speed of the mean solar wind. The method applies to heliocentric ranges from 3 to about 10 $R_\odot$ in the region surrounding the plasma sheet. To implement the diagnosis, we first establish the connection between the Alfvén speed and the observed phase speed, then we put constraints on the solar wind velocities with blob measurements, and determine the density distributions through the inversion of the LASCO pB data. The obtained profiles of the magnetic field strength are in line with other estimates in the corona.

Previous studies indicate that the magnetic flux tube experiences a dramatic expansion in the neighborhood of the streamer cusp and a possible contraction beyond (e.g., Wang 1994; Bravo & Stewart 1997; Chen & Hu 2001, 2002; Hu et al. 2003; Li et al. 2006). Till now, there exist no direct observational proofs of the above peculiar feature of the magnetic field near the streamer cusp. From the seismological study of this paper, we see that the magnetic field along the plasma sheet expands more or less radially starting from as near as 3 $R_\odot$. Therefore, the above-mentioned intriguing expanding process of the flux tube occurs, if it does, below this distance. This provides observational constraints on relevant models.

According to our seismological studies on the basis of speed measurements of the two wave phases, we find that the Alfvén speed and magnetic field strength at a fixed distance decrease with time. This has been suggested to be a result of the recovering process of the CME-disturbed corona. In the process, the magnetic field initially stretched out by the CME ejecta may get relaxed through processes like magnetic reconnections, and the evacuated corona may get refilled gradually through plasma heating and resultant expansions. As mentioned in the previous section, the occurrence of this dynamic recovering process contributes directly to the uncertainty of our results, since we have adopted identical and steady solar wind parameters for the diagnoses associated with the two phases. Due to the lack of direct measurements on these parameters in the near-Sun region, it is currently not possible to evaluate the impact of using time-dependent solar wind parameters on our results.

Apart from the indeterminacy associated with solar wind densities and velocities, there exist two other major factors contributing to our diagnostic uncertainties. One is the error coming from the phase speed measurements, which was already discussed and estimated to be about ±10% (or ±50 km s^{-1}) in Paper I. This error will be passed directly to the evaluation of the Alfvén speed and the magnetic field strength. Another factor stems from the approximate relationship between the kink mode and the external Alfvén speed. In the paper, the relationship was determined with the dispersion relation given by Edwin & Roberts (1982) for a simplified magnetized plasma slab configuration under Cartesian coordinates. This geometry is different from the realistic spherical, inhomogeneous (both in the radial and latitudinal directions), and time-dependent

streamer-plasma-sheet configuration. Therefore, future studies should investigate the properties of the kink mode under more realistic geometry. In addition, theoretical and numerical efforts should continue to explore excitation conditions and propagation properties of streamer waves in the process of CME–streamer interaction, and determine the connection between the wave properties and the background plasma properties. These works will be of great benefit to future seismological studies with streamer waves.

The *SOHO*/LASCO data used here are produced by a consortium of the Naval Research Laboratory (USA), Max-Planck-Institut für Aeronomie (Germany), Laboratoire d'Astronomie Spatiale (France), and the University of Birmingham (UK). *SOHO* is a project of international cooperation between ESA and NASA. We thank Dr. A. Vourlidas for helping us analyze the LASCO pB data. This work was supported by grants NNSFC 40774094, 40825014, 40890162, a Special Fund for Public Welfare Industry (meteorology): GYHY200806024, and a Foundation for the Author of National Excellent Doctoral Dissertation of PR China (2007B24). B.L. is supported by the grant NNSFC 40904047, and L.D.X. by 40774080 and 40974105.

APPENDIX

DISPERSION DIAGRAMS OF THE FAST KINK BODY MODE AND THE RELATIONSHIP OF v_k AND v_{Ae}

To determine the relationship between the phase speed of the fast kink body mode and the Alfvén speed, we conduct a parameter study on the dispersion relation in a slab configuration of magnetized plasmas under local approximations (Equation (11) of Edwin & Roberts 1982), which is written as

$$n_e(k^2v_{Ae}^2-\omega^2)m_0\coth(m_0x_0)+n_0(k^2v_{A0}^2-\omega^2)m_e=0,$$

where $\omega(k)$ is the wave frequency (number) and x_0 is the half-width of the slab. The subscript "0" ("e") represents parameters for interior (exterior) of the plasma slab, n being the number density, and the Alfvén speed $v_{A0,e}=\frac{B_{0,e}}{\sqrt{\mu_0 m_p n_{0,e}}}$. The sound speed $c_{s0,e}=\sqrt{\frac{2\gamma k_B T_{0,e}}{m_p}}$ is implicitly contained in the expressions of m_0 and m_e whose definitions are given in the above paper. In our study, the polytropic index γ is taken to be 1.1 to calculate the sound speeds in the heated coronal environment. For the fast kink body mode, it is required that ${m_0}^2<0$ and $m_e>0$. To solve the dispersion relation and to find out the relationship between the observed phase speed and the Alfvén speed, it is necessary to specify all coronal parameters required in the above dispersion relation, including number densities, plasma temperatures, and magnetic field strengths both inside and outside of the slab structure of the plasma sheet. Different sets of coronal parameters at three nominal heliocentric distances (3, 5, and 7 $R_\odot$) are specified based on available observational diagnoses and theoretical modelings.

The electron number density along a streamer axis was given by many other authors using the inversion method of the LASCO pB data (e.g., Strachan et al. 2002, Uzzo et al. 2006). For the specific streamer in question, we take advantage of the pB inversion program enclosed in the Solar Software system (SSW) to give the electron density profile along the axis, which is taken to be the density inside the slab n_0. The obtained density profile has been presented in Figure 2. Here, we repeat the density values which are 7.19×10^5 (1.67×10^5) cm^{-3} at 3 (5) $R_\odot$. The density at 7 $R_\odot$ is estimated to be 8.5×10^4 cm^{-3} by assuming an r^{-2} dependence with r representing the heliocentric distance. The electron density outside the sheet n_e is given by half of the interior densities at the same height for simplicity.

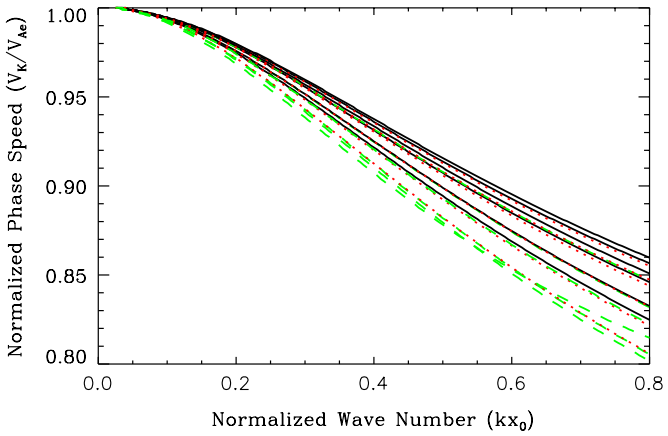

Figure 4. Eighteen dispersion curves of the fast kink body mode using various sets of prescribed coronal parameters with the solid-black (dotted-red, dashed-green) lines corresponding to parameters for the nominal distance of 3 (5, 7) $R_\odot$, see the Appendix for details.

(A color version of this figure is available in the online journal.)

The temperature required to solve the dispersion relation is the average of the proton and electron temperatures since the slab model makes use of a single-fluid approximation. There exist certain measurements on the kinetic temperatures (sum of the thermal temperature and the contribution due to turbulent motions) of protons along the streamer axis from about 1.75 $R_\odot$ to 5 $R_\odot$ (e.g., Strachan et al. 2002; Uzzo et al. 2006), which indicate that the proton kinetic temperature decreases slowly with radial distance from 1.58 MK at 3 $R_\odot$ to 1.24 MK at 5 $R_\odot$. However, no electron temperature measurements are available beyond 1.5 $R_\odot$ in the corona. Nevertheless, there are numerical endeavors which manage to produce electron temperature profiles in the solar wind along the streamer plasma sheet (e.g., Chen & Li 2004; Li et al. 2006). These models show that the electron temperature also decreases slowly from a value larger than 1 MK at the coronal base to 4–6×10^5 K at about 10 $R_\odot$. Keeping these numbers in mind, we adopt two sets of temperature profiles for the parameter study on the dispersion relation: one set is for isothermal temperature profiles (being 1 MK everywhere) and the other set is for an r^{-1}-dependent temperature profile with a prescribed value of 1.2 MK at 3 $R_\odot$.

Regarding the magnetic field strength, from the Faraday rotation measurement of extragalactic radio sources, Ingleby et al. (2007) gave an estimate of about 0.05 G at 5 $R_\odot$ "outside of the region around the neutral line," or in other words, outside the streamer current-plasma sheet region. For our study, we take their result to give one set of values of magnetic field strength outside of the plasma sheet, i.e., B_e. Besides, we also use two other field strengths at 5 $R_\odot$ different from their value by $\pm25\%$, respectively. The field strengths at the rest of the nominal distances are given using the r^{-2} dependence. The magnetic field strength inside the plasma sheet B_0 is calculated from the total-pressure balance condition.

The yielded 18 dispersion curves are plotted all together in Figure 4 with the solid-black (dotted-red, dashed-green) lines corresponding to the nominal distance of 3 (5, 7) $R_\odot$. The ordinate is the kink mode phase speed v_k normalized by v_{Ae}, the abscissa is the dimensionless wave number kx_0 with k being the radial wave number, and x_0 being the half-width

of the plasma sheet, as already defined. It can be seen that $v_k \approx v_{Ae}$ with a long wavelength or small kx_0, and v_k decreases monotonically with increasing kx_0. The values of k and x_0 for the concerned event will be specified in the following paragraph.

In situ detections indicate that the angular width of the plasma sheet structure is less than 3° (Borrini et al. 1981; Goldstein et al. 1996); this is consistent with coronagraph observations. In Figure 2(a), we show the pB data obtained by LASCO on 2004 July 5, one day prior to the streamer wave event. The two arcs are at the heliocentric distances of 4 and 5 $R_\odot$, the pB data along which are shown in Figure 2(b). The data are normalized by corresponding maximum pB values. We see that 3° is an appropriate value for the angular width of the plasma sheet, through which the width of the plasma sheet at a certain heliocentric distance can be easily determined. The wave numbers $k = 2\pi/\lambda$ can be calculated given the wavelengths λ being 2.0 (2.1, 2.4) $R_\odot$ at 3 (5, 7) $R_\odot$ according to Paper I. We then have $kx_0 = 0.25$, 0.39, and 0.48 for the three distances. We see that the corresponding ratio of v_k/v_{Ae} $(= \alpha)$ varies in a small range from 0.97 to 0.88, apparently insensitive to the changing parameters.

From further calculations (not included in this paper), it is clear that using other reasonable parameters in between, or lower than the above two sets of temperatures, larger field strengths, or smaller outside densities result in no observable effect on the final value of α. This is actually a result of a property of the solved dispersion relation of the fast kink body mode: as long as v_{Ae} is larger than all other characteristic speeds present in the dispersion relation, the phase speed of the mode is smaller yet rather close to v_{Ae}, i.e., α is smaller yet rather close to unity. This allows us to adopt a uniform approximate relationship of v_{Ae} and v_k for different coronal parameters: $v_{Ae} = v_k/\alpha$, where α is fixed to be a constant of 0.92 according to the above parameter study. Once the value of α is decided, the Alfvén speed in the region outside of the plasma sheet can be easily deduced. However, it should be noted that the actual morphology of the streamer plasma sheet is more complex than the slab model used here. Therefore, the work presented is expected to be improved by future wave analysis considering some more realistic configurations.

REFERENCES

Borrini, G., Wilcox, J. M., Gosling, J. T., Bame, S. J., & Feldman, W. C. 1981, J. Geophys. Res., 86, 4565
Bravo, S., & Stewart, G. A. 1997, ApJ, 489, 992
Chen, Y., & Hu, Y. Q. 2001, Sol. Phys., 199, 371
Chen, Y., & Hu, Y. Q. 2002, Ap&SS, 282, 447
Chen, Y., & Li, X. 2004, ApJ, 609, L41
Chen, Y., Li, X., Song, H. Q., Shi, Q. Q., Feng, S. W., & Xia, L. D. 2009, ApJ, 691, 1936
Chen, Y., Song, H. Q., Li, B., Xia, L. D., Wu, Z., Fu, H., & Li, X. 2010, ApJ, 714, 644
Cho, K.-S., Lee, J., Gary, D. E., Moon, Y.-J., & Park, Y. D. 2007, ApJ, 665, 799
Dulk, G. A., & McLean, D. J. 1978, Sol. Phys., 57, 279
Edwin, P. M., & Roberts, B. 1982, Sol. Phys., 76, 239
Goldstein, B. E., et al. 1996, A&A, 316, 296
He, H., & Wang, H. N. 2008, J. Geophys. Res., 113, A05S90
Hu, Y. Q., Habbal, S. R., Chen, Y., & Li, X. 2003, J. Geophys. Res., 108, 1377
Ingleby, L. D., Spangler, S. R., & Whiting, C. A. 2007, ApJ, 668, 520
Li, B., Li, X., & Labrosse, N. 2006, J. Geophys. Res., 111, A08106
Linker, J. A., et al. 1999, J. Geophys. Res., 104, 9809
Mancuso, S., & Spangler, S. R. 1999, ApJ, 525, 195
Mancuso, S., & Spangler, S. R. 2000, ApJ, 539, 480
Pätzold, M., Bird, M. K., Volland, H., Levy, G. S., Seidel, B. L., & Stelzried, C. T. 1987, Sol. Phys., 109, 91
Ramesh, R., Kathiravan, C., & Sastry, Ch. V. 2010, ApJ, 711, 1029
Sakurai, T., & Spangler, S. R. 1994, ApJ, 434, 773
Sastry, Ch. V. 2009, ApJ, 697, 1934
Schatten, K. H., Wilcox, J. M., & Ness, N. F. 1969, Sol. Phys., 6, 442
Schrijver, C. J., & Derosa, M. L. 2003, Sol. Phys., 212, 165
Sheeley, N. R., Jr., et al. 1997, ApJ, 484, 472
Smerd, S. F., Sheridan, K. V., & Stewart, R. T. 1974, in IAU Symp. 57, Coronal Disturbances, ed. G. A. Newkirk (Dordrecht: Reidel), 389
Smerd, S. F., Sheridan, K. V., & Stewart, R. T. 1975, Astrophys. Lett., 16, 23
Song, H. Q., Chen, Y., Liu, K., Feng, S. W., & Xia, L. D. 2009, Sol. Phys., 258, 129
Spangler, S. R. 2005, Space Sci. Rev., 121, 189
Strachan, L., Suleiman, R., Panasyuk, A. V., Biesecker, D. A., & Kohl, J. L. 2002, ApJ, 571, 1008
Uzzo, M., Strachan, L., Vourlidas, A., Ko, Y. K., & Raymond, J. C. 2006, ApJ, 645, 720
Vrsnak, B., Magdalenic, J., Aurass, H., & Mann, G. 2002, A&A, 396, 673
Wang, Y.-M. 1994, ApJ, 437, L67
Wang, Y.-M., Sheeley, N. R., Jr., Socker, D. J., Howard, R. A., & Rich, N. B. 2000, J. Geophys. Res., 105, 25133
Wang, Y.-M., et al. 1998, ApJ, 498, L165
Wiegelmann, T. 2008, J. Geophys. Res., 113, A03S02
Yan, Y. H., & Sakurai, T. 2000, Sol. Phys., 195, 89